Control of the Discrete Vortices from a Delta Wing

Mohamed Gad-el-Hak*
University of Notre Dame, Notre Dame, Indiana
and
Ron F. Blackwelder†
University of Southern California, Los Angeles, California

In a previous study, a series of flow visualization experiments indicated that the classical leading edge vortices on delta wings originate as a series of discrete vortices that are shed from the leading edge at a well-defined frequency. Inspired by the recent attempts to control the growth rate of a free shear layer by perturbing the flow at the end of the splitter plate, a novel method was used in the present investigation to control these discrete vortices. The flow was perturbed by impulsively injecting or withdrawing secondary fluid from a slot along the entire leading edge of a delta wing. The frequency of perturbation and the flow rate from the slot were varied over a wide range. The experiments were conducted in both a water towing tank and a wind tunnel, and flow visualization and velocity probe measurements were used to assess the perturbation effects on the flowfield. The instantaneous velocity signal was used to compute the important statistical quantities of the random velocity field, such as the mean, the root mean square, the spectral distribution, the auto- and cross-correlations, and the probability density function. Over a wide range of Reynolds numbers and angles of attack, the present probe measurements further validated the discrete nature of the leading edge vortices. Moreover, leading-edge perturbations dramatically affected the evolution of the bounded shear layer originating from the delta wing's leading edge. It is found that maximum changes in the leading edge vortices occur when the perturbation frequency is a subharmonic of the natural shedding frequency of the unperturbed wing and when the injection/suction speed is about the same order of magnitude as that of the ambient velocity.

Nomenclature

A_j	= area of leading edge slot
A_w	= area of delta wing
AR	= aspect ratio
c	= root chord
f	= perturbation frequency
f_0	= natural shedding frequency
$P(U)$	= probability density function of the streamwise velocity
R_c	= chord Reynolds number, $U_\infty c/\nu$
$R(\tau)$	= autocorrelation coefficient
$S(f)$	= normalized power spectral density
$S'(f)$	= dimensional power spectral density, $\overline{u^2}S(f)$
s	= wing semispan
t	= time, s
U_j	= injection (suction) speed
U_∞	= towing speed
$U(t)$	= instantaneous streamwise velocity
$\overline{U}(x,y,z)$	= mean longitudinal velocity
$u(x,y,z,t)$	= streamwise velocity fluctuations, $U-\overline{U}$
$\sqrt{\overline{u^2}}$	= root mean square of longitudinal velocity fluctuations
x,y,z	= Cartesian coordinates fixed with the wing
α	= angle of attack
β	= apex angle
ν	= kinematic viscosity
τ	= correlation time interval
ρ	= fluid density

Received June 4, 1986; presented as Paper 86-1915 at the AIAA 10th Aeroacoustics Conference, Seattle, WA, July 9-11, 1986; revision received Nov. 10, 1986.

*Professor of Aerospace and Mechanical Engineering. Member AIAA.
†Professor of Aerospace Engineering. Member AIAA.

I. Introduction

WITH the recent advances in short-range infrared guided missiles, a significant change in close air combat characteristics emphasizing sudden maneuverability has become necessary. This has led to a growing interest in the so-called "supermaneuverability" of fighter aircraft, which attempts to utilize regions of the maneuver envelope that have been unattainable historically, such as post-stall flight maneuver and side slipping.[1,2] Both improvements to existing vortex control methods and the development of novel devices may help achieve the desired high degree of maneuverability.

The flow over a delta wing at a constant angle of attack is dominated by two large-bound vortices that result from the flow separation at the leading edge.[3-7] With a sharp leading edge at an angle of attack α, the flow is separated along the entire leading edge forming a strong shear layer. The shear layer is wrapped up in a spiral fashion, which results in a large-bound vortex on each side of the wing. The two vortices appear on the suction surface of the wing in the form of an expanding helix when viewed from the apex of the lifting surface. The low pressure associated with the vortices produces additional lift on the wing, often called nonlinear or vortex lift, which is particularly important at large angles of attack.

Recently, the present authors[8] conducted a series of flow visualization experiments that indicated that the leading-edge vortex on a delta wing at a *constant* angle of attack consists of a series of *discrete* smaller vortices. These vortices are shed parallel to the leading edge at a repeatable frequency, and their trajectories follow the general outline of the classical large-bound vortex on each side of the wing. As the discrete vortices follow this course, two vortices appear to roll around each other and merge to form a single larger vortex, much the same as has been observed in a free shear layer originating at a splitter plate between two streams of

differential velocity.[9-11] This process was observed to repeat itself several times culminating in the large-bound vortex.

Inspired by the recent research to control the growth rate of free shear layers,[12] the present paper reports on preliminary attempts to modulate the shedding and the pairing of the discrete vortices. The flow at the leading edge of the delta wing was perturbed by impulsively injecting at constant frequency a secondary fluid from a slot along that edge. The flowfield was altered significantly when the injection frequency was chosen to be a subharmonic of the shedding frequency of the discrete vortices. The injection of secondary fluid may be useful as a means of controlling the development and strength of the bound edge vortices on delta wings.

In this study, experiments were conducted in both a water towing tank and a wind tunnel to characterize the flowfield around a delta wing with and without the influence of the vortex control device. Flow visualizations and velocity surveys using fast-response probes were conducted. Important statistical quantities of the random velocity field were computed to further validate our previous flow visualization results regarding the discrete nature of the leading edge vortices and to assess the effects of the leading edge excitations on the shear layer associated with the discrete vortices.

II. Experimental Approach

Towing Tank

The flow visualization tests were conducted in an 18-m-long, 1.2-m-wide, and 0.9-m-deep towing tank.[13] The delta wing was sting mounted on a carriage that rode on two tracks located on top of the towing system. During towing, the carriage was supported by an oil film, which ensured a vibrationless tow. The equivalent freestream turbulence was checked using a hot-film probe and was found to be about 0.1% of the mean towing speed. The carriage was towed by two cables driven through a reduction gear by a 1.5-hp Boston Ratiotrol motor. The towing speed was regulated within an accuracy of 0.1%. The system was able to achieve towing speeds between 1 and 300 cm/s, yielding a chord Reynolds number in the range of $R_c = 2.5 \times 10^3 - 7.5 \times 10^5$.

Wind Tunnel

The Venturi wind tunnel located at the University of Washington's Department of Aeronautics and Astronautics was used to measure the velocity field about the delta wing. The test section has a hexagonal cross section 1 m wide, 0.8 m high, and 1 m long. The wind tunnel is powered by a 10-hp dc motor driving a 1.6-m, four-bladed propeller located approximately 4 m downstream of the test section. The model was mounted in the test section using a three-point support system consisting of two fixed bayonets forward and a pitch arm aft. The maximum speed of the tunnel was 25 m/s ($R_c \equiv U_\infty c/\nu = 6.7 \times 10^5$) with the model installed. The background turbulence in the tunnel was quite high and exceeded 1% in spite of the addition of several turbulence management devices (honeycombs, screens, etc.).

Delta Wing Models

Two different delta wing models were used in the present investigation. For the flow visualization experiments conducted in the water tank, a delta wing with a sharp leading edge, a root chord of 25 cm and a sweep of 60 deg ($\beta = 60$ deg) was used. A larger model having a root chord of 40 cm, a 60-deg sweep angle, and a sharp leading edge was used in the wind tunnel tests. Both models were machined from Plexiglas and were sting mounted so that their angle of attack varied in the range of 0 to 40 deg.

Leading Edge Excitation

To perturb the shear layer originating at the leading edge of a delta wing, a variety of methods are available:

1) A passive cavity system tuned to a frequency range corresponding to the natural frequency of the vortex shedding.

2) Acoustical means such as the use of an array of speakers along the leading edge of the wing.

3) A piezoelectric array embedded in the wing near the leading edge.

4) A heating element to provide an unsteady perturbation to the flow before separation.

5) Blowing and/or sucking through slots in the leading edge.

6) Mechanical devices, such as a vibrating ribbon, etc.

In this preliminary investigation, only method 5 was tested. Periodic blowing or suction was applied through both leading edges of the delta wing models. A uniform slot 0.2 mm wide was formed at each leading edge and plumbed to a system of small conduits inside the model.

In the towing tank experiments, a constant head tank was used together with a solenoid valve to inject water and/or dye at a given frequency and amplitude out of the leading edge slots. The solenoid valve was driven by a square-wave signal generator having the desired frequency. After passing through the solenoid valve, the dyed water entered the delta wing through the main sting at the midpoint of the trailing edge. It passed through several small conduits to an internal reservoir directly behind the 0.2-mm-wide slot. This ensured that the enjection was uniform to within $\pm 2\%$ along the leading edge.

In the wind-tunnel tests, a 100-psi compressed-air line was used to inject air periodically through the leading-edge slots in the model. The secondary air flowrate was varied using a pressure regulator, and the perturbation frequency was controlled using a specially fabricated rotary valve driven by an external motor. The same valve was used together with a vacuum chamber to achieve periodic suction in the wind-tunnel experiments.

The peak ejection or suction speeds from the leading edge slots varied over the wide range of 0 to $2U_\infty$. While the upper limit of this range may seem excessive, the resulting mass flux was still small because of the extremely small area of the leading-edge slot compared to the area of the delta wing ($1/2\rho U_j^2 A_j \ll 1/2\rho U_\infty^2 A_w$).

Flow Visualization Methods

The water towing tank was used to conduct flow visualization experiments to assess the nature of the discrete vortices shed from a delta wing with and without the leading-edge excitations. Food color and fluorescent dyes were used in the present investigation. The food color dyes, illuminated with conventional floodlights, were used to obtain overall views of the flowfield as recorded by a camera mounted on top of the towing tank. The fluorescent dyes were excited with sheets of laser light projected in the desired plane. To produce a sheet of light, a 5-W argon-ion laser (Spectra Physics, Model 164) was used with a mirror mounted on an optical scanner having a 720-Hz natural frequency (General Scanning, Model G124). A sine-wave signal generator, set at a frequency equal to the inverse of the camera shutter speed, drove the optical scanner to produce light sheets approximately 1 mm thick.

Side views of the flowfield were obtained using a vertical sheet of laser light in the x-y plane at $z = 10$ cm and a camera towed with the wing but located outside the tank. (The Cartesian coordinates system used is fixed with the wing and has its origin at the apex of the delta wing; x is along the root chord and y is normal to the model surface.) End views were obtained using a vertical sheet of laser light in the y-z plane at $x = 20$ cm (80% of the root chord) and an underwater camera towed behind the wing using the same carriage.

Velocity Probes

To further validate our previous flow visualization results regarding the discrete nature of the leading edge vortices and to quantitatively determine the effects of leading-edge excitations on the bounded shear layer, hot-film and hot-wire

probes were used to survey the velocity field around the delta wing mounted in the Venturi wind tunnel. Miniature, single-element probes (TSI Model 1260) having a diameter of 0.025 mm and a sensing length of 0.25 mm were used. A three-dimensional traverse was used to survey the longitudinal velocity fluctuations in the vicinity of the delta wing. The probe position was ascertained by recording the relative distance between the leading edge at a fixed x/c location and the sensor. The positional uncertainties in x,y, and z directions were 1.0, 0.3, and 0.3 mm, respectively. Conventional turbulence statistics such as the mean, root mean square, spectrum, correlation, and probability distribution were computed from the velocity signals.

The fast-response probe signals were first recorded on an instrumentation tape recorder (Hewlett-Packard Model 3964A). The FM analog tape recorder had four channels, used 6 mm tape and had a frequency bandwidth from dc to 5 kHz. The data were stored in the analog tape and digitized later using the analog-to-digital converter on a NOVA 800 minicomputer. The instantaneous velocity signals were obtained by linearization using a fourth-order polynomial and the data were stored on digital tape. Subsequent data analysis was performed on the NOVA and on a PRIME P750 computer.

Considerable care is necessary to interpret the hot-wire signals in the present investigation because the mean flowfield is strongly three-dimensional. For example, consider a traverse across the wing parallel to the z axis. Outside the leading edge, the sensor first sees a flow parallel to the x axis, i.e., perpendicular to the sensor's axis. Near the leading edge, and especially at small y values, the sensor encounters a strong shear layer with a thickness comparable to the sensor's length. As z is decreased further, the primary separated region of the bound vortex is encountered, followed by a region of secondary separation, the three-dimensional flow of the vortex, etc. Consequently the signals from the hot-wire anemometer are due not only to the streamwise velocity component, but also have contributions from the other two velocity components as well. No attempt was made to resolve these components in the present preliminary investigation.

III. Flow Visualization Results

Photographs illustrating the discrete vortices shed from the leading edge of a delta wing were presented by Gad-el-Hak and Blackwelder[8] for the unperturbed case. They observed that the vortices are shed parallel to the leading edge and rotate around each other and pair to form larger vortices while simultaneously moving downstream. As depicted by Winant and Browand[9] and Roshko[11] for a two-dimensional free shear layer originating at a splitter plate between two streams of differing velocity, the pairing process is an important contributor to the growth of the vortical region. Although the present flow is three-dimensional and bounded on one side by the surface of the wing, it is nevertheless a shear layer and its evolution is governed by the same physical processes that influence the classical mixing layer.

Although observed at all angles of attack in the range of 0 to 40 deg, the best attack angle to visualize the shedding from the delta wing and subsequent pairing of the discrete vortices was in the range of 10 to 15 deg. At angles below 5 deg, the pairing process seemed to be inhibited by the proximity of the solid boundary. At larger angles of attack, the flow was more turbulent and masked the observed phenomenon. The shedding frequency depended on both the angle of attack and the flow speed. For example, at $\alpha = 15$ deg, Gad-el-Hak and Blackwelder[8] presented the following empirical formula for the natural shedding frequency f_0 as a function of the chord Reynolds number R_c:

$$f_0 c/U_\infty = 1625/\sqrt{R_c}$$

where c is the root chord and U_∞ is the freestream speed.

By perturbing the leading edge of a delta wing, the shedding and the pairing of the discrete vortices were modulated much the same as the changes in the growth rate achieved in perturbed free shear layers.[12] End views depicting the unperturbed and perturbed flowfields are shown in the sequence of photographs in Figs. 1 and 2, respectively. The sharp leading-edge delta wing was at an angle of attack of $\alpha = 10$ deg and had a chord Reynolds number of $R_c = 1.25 \times 10^4$. In the perturbed case (Fig. 2), the flow at the leading edge was disturbed by a square-wave excitation with a peak ejection speed equal to the towing speed ($U_j = U_\infty = 5$ cm/s) and a frequency equal to one-half the natural shedding frequency ($f = 0.5 f_0 = 1.1$ Hz). The perturbed shear layer seen in the ciné films (available upon request) was quite different from

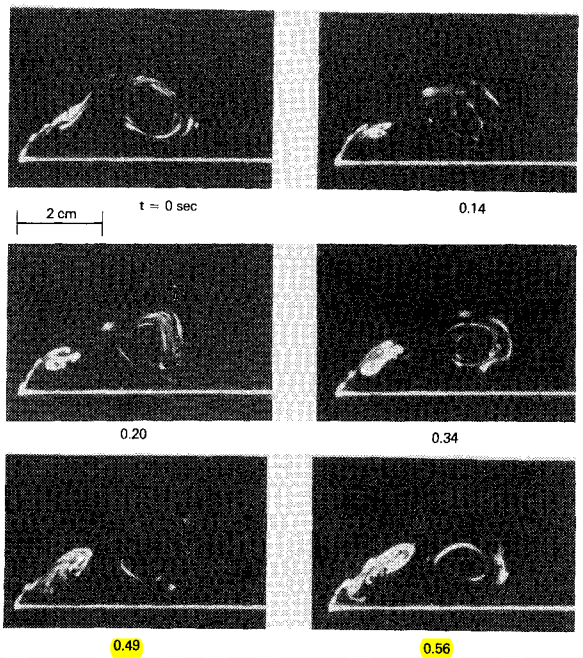

Fig. 1 End view of the discrete leading edge vortices: $R_c = 1.25 \times 10^4$; $\alpha = 10$ deg. Natural shedding frequency $f_0 = 2.2$ Hz.

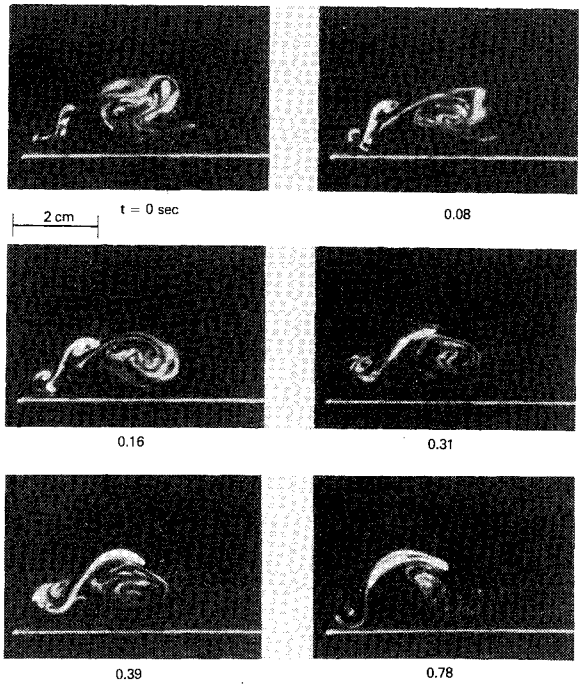

Fig. 2 End view. Subharmonic perturbations applied at the leading edge. Pairing is enhanced and the large vortex is more organized.

the natural one. The first pairing was more repeatable and occurred closer to the leading edge. After the dye had spread to fill the entire leading-edge vortex, the dyed area was 30% larger than the similar area observed in the unperturbed case.

The results from higher injection rates were more difficult to interpret. The pairing process was not enhanced and less regular when $U_j = 2U_\infty = 10$ cm/s. In addition, the resulting large vortex was less organized, displayed a more random character and appeared to occupy a larger volume (i.e., the dye was more disperse). Similar results were noted at the same ejection velocity when the frequency was halved to one-quarter of the natural shedding frequency.

In summary, the visualization experiments indicate that the classical large vortices on a delta wing originate as a series of smaller vortices shed from the leading edge and parallel to it. The pairing process between these vortices is dynamically significant and can be modulated by perturbing the leading edge of the wing. Weak subharmonic perturbations seem to enhance the pairing and result in a more organized large vortex.

IV. Velocity Measurements

The large delta wing model was tested in the Venturi wind tunnel to obtain velocity measurements. The root-chord Reynolds number in the experiment was varied over the range of 1×10^5 to 4×10^5 by controlling the freestream velocity. Miniature, single-element hot-wire probes were used to survey the instantaneous longitudinal velocity at different positions within the leading-edge vortices and at different run conditions.

The coordinate system used had its origin at the apex of the delta wing; x was along the root chord, y was normal to the model surface, and z was in the spanwise direction. Measurements were conducted at the attack angles of 10 and 28 deg, at two streamwise stations, $x/c = 0.3$ and 0.6, and at different y and z locations. The complex, three-dimensional shear layer was investigated without perturbation, with periodic injection at the leading edge and with periodic suction.

Samples of the instantaneous, unperturbed longitudinal velocity signal, normalized with the tunnel speed, are shown in Fig. 3 for a Reynolds number of $R_c = 1.3\times10^5$ and an angle of attack $\alpha = 28$ deg. The measurements were conducted along the $x = 0.6c$ plane at $y = 0.01c$, where c is the root chord. Four different spanwise positions are shown in the figure: $z/c = 0.349$, 0.346 (leading edge), 0.344 and 0.326. All four positions are very close to the leading edge, yet dramatic differences exist between each time record, consistent with the presence of an intense shear layer.

At the most outboard position, $z/c = 0.349$, the mean flow velocity exceeds U_∞ due to the acceleration around the leading edge. The negative spikes in the instantaneous streamwise velocity are consistent with the passing of the discrete vortices at the fixed probe location. As these vortices rotate, lower-speed fluid is transported to the high-speed side of the shear layer. A well-defined mean shedding frequency is apparent and was computed from the spectrum peak of the raw velocity data (Sec. VI). The negative spikes are still apparent at $z/c = 0.346$ but are now embedded in the background turbulence and the mean speed is lower. Positive spikes are observed as the probe is traversed inward from the leading edge ($z/c = 0.344$ and 0.326), and the mean speed continues to drop indicating a strong spanwise shear.

Similar velocity records were obtained at other angles of attack and other Reynolds numbers. These results further confirmed our previous flow visualization findings regarding the discrete nature of the leading-edge vortices.

The longitudinal mean velocity profile as function of spanwise distance is shown in Fig. 4 for the same run conditions depicted in Fig. 3. At the centerline of the delta wing ($z/c = 0$), the velocity near the surface is twice that of the

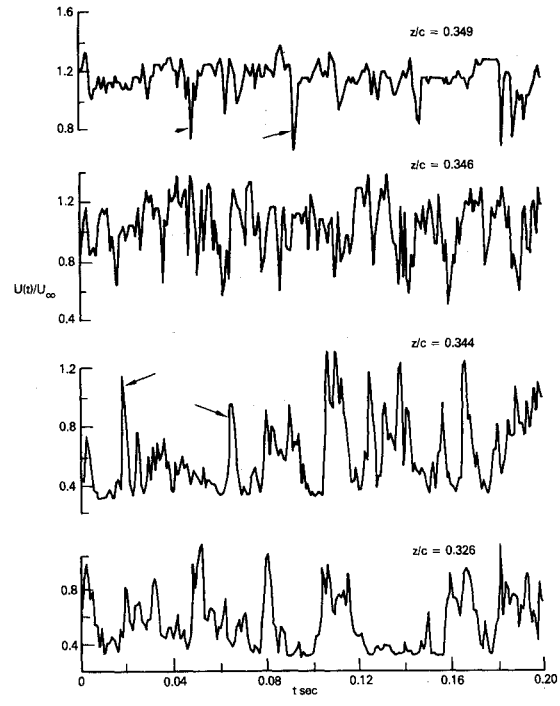

Fig. 3 Instantaneous longitudinal velocity records: $x/c = 0.6$; $y/c = 0.01$; $R_c = 1.3\times10^5$; $\alpha = 28$ deg; $U_j/U_\infty = 0$.

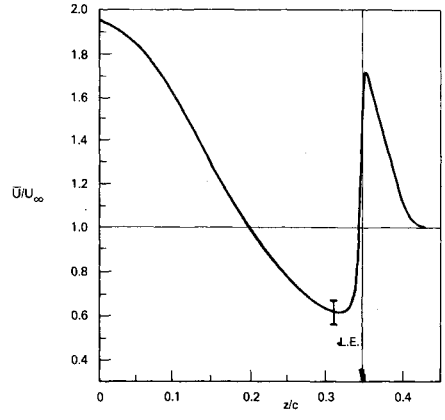

Fig. 4 Longitudinal mean velocity profile: $x/c = 0.6$; $y/c = 0.01$; $R_c = 1.3\times10^5$; $\alpha = 28$ deg; $U_j/U_\infty = 0$.

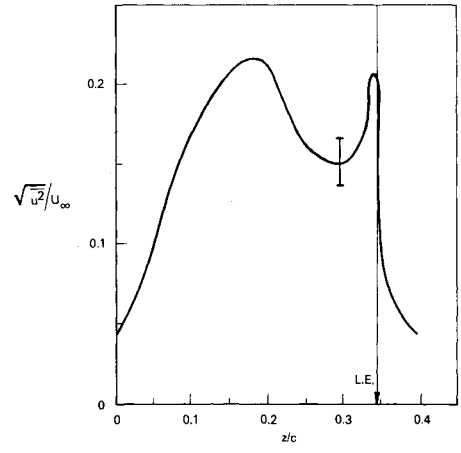

Fig. 5 Root mean square velocity fluctuations: $x/c = 0.6$; $y/c = 0.01$; $R_c = 1.3\times10^5$; $\alpha = 28$ deg; $U_j/U_\infty = 0$.

ambient speed. It drops to a low of $0.6U_\infty$ at $z/c=0.3$ just inward of the leading edge, and decays to U_∞ further out. This strong shear region illustrates the strength of the leading-edge shear layer and is the location where the discrete vortices are pairing and interacting dynamically.

The root mean square (rms) profile obtained for the same signal is shown in Fig. 5 normalized with the tunnel speed U_∞. The two peaks in the velocity fluctuations correspond to the positions of maximum shear seen in Fig. 4. The maximum rms is 27% of the local mean velocity $\overline{U}$ at these regions of intense shear.

The mean and rms velocity profiles at four different heights above the suction surface of the perturbed delta wing are shown in Figs. 6 and 7 for the same Reynolds number and attack angle as in Figs. 4 and 5. Subharmonic excitations were applied at the leading edge of the wing with $U_j=1.73\ U_\infty$, and the spanwise profiles are taken at $x/c=0.6$ and $y/c=0.01$, 0.03, 0.05, and 0.08. It is clear from these four profiles that the shear layer is extremely complex.

At $y/c=0.01$, a direct comparison between the perturbed (Figs. 6 and 7) and the unperturbed (Figs. 4 and 5) cases is possible. The perturbation dramatically alters the mean and rms velocity distributions. The mean velocity peak near the leading edge drops from $1.8U_\infty$ in the unperturbed case to $1.3\ U_\infty$ in the excited flow. The inboard maximum also seems to be reduced. The region where $\overline{U}<U_\infty$ is almost eliminated by the ejection disturbance. Thus a substantial change in the vortex structure has obviously occurred, suggesting that the circulation has been altered as well.

A similar dramatic change in the fluctuating velocity at $y/c=0.01$ is seen by comparing Figs. 5 and 7. Although the peak value near the leading edge has the same magnitude, the inboard rms values are reduced significantly, i.e., from $0.2U_\infty$ to roughly $0.05U_\infty$ at $z/c=0.2$. The fluctuations at $y/c\geq 0.03$ (Fig. 7) suggest that the amplitude rises further inboard; nevertheless, a large alteration of the flow seems evident.

The relative effect of suction vs ejection is seen in Figs. 8 and 9. The mean and rms profiles are depicted for three cases: no perturbation; subharmonic ejection ($U_j=1.73U_\infty$); and subharmonic suction ($U_j=-0.87U_\infty$), where U_j is the peak injection speed from the leading-edge slot. The Reynolds number in all three cases is $R_c=1.3\times10^5$, the angle of attack is 28 deg, and the spanwise profiles are taken at $x/c=0.3$ and $y/c=0.003$. The leading-edge perturbations shift the interface of the shear layer inward toward the wing centerline. The maximum speed near the leading edge is not affected, but the minimum speed is dramatically reduced by the periodic suction or ejection. Both the mean and rms profiles appear to be more complex in the case of subharmonic suction perturbation. Note that the second peak in the rms profiles is not quite developed at this upstream station ($x/c=0.3$) compared to the location further downstream, e.g., $x/c=0.6$ in Figs. 5 and 7. These figures also show that the effect of the suction/ejection is more dramatic at $x/c=0.6$.

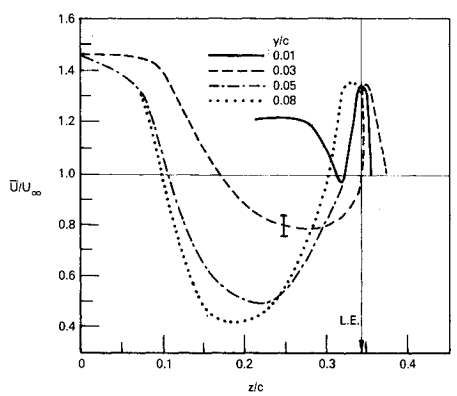

Fig. 6 Mean velocity profiles in the perturbed case: $x/c=0.6$; $R_c=1.3\times10^5$; $\alpha=28$ deg; $U_j/U_\infty=1.73$.

V. Probability Distribution

A useful statistical quantity that may shed some light on the phenomenon of discrete vortices and the effects of leading edge perturbations on the shear layer is the probability density function of the streamwise velocity fluctuations,[14,15] which is a measure of the relative amount of time that the velocity $U(t)$ spends at various levels. We start with

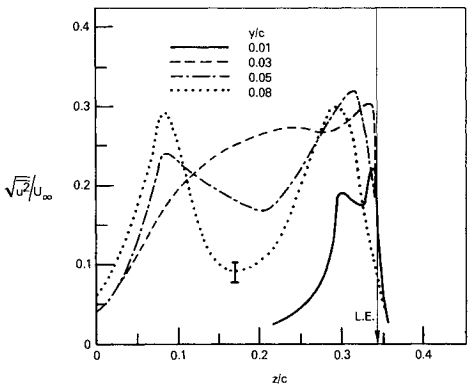

Fig. 7 Root mean square velocity fluctuations in the perturbed case: $x/c=0.6$; $R_c=1.3\times10^5$; $\alpha=28$ deg; $U_j/U_\infty=1.73$

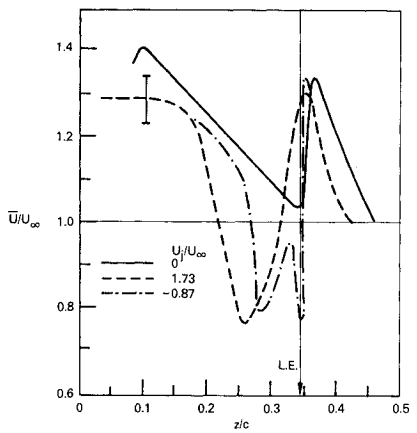

Fig. 8 Effects of suction and ejection on the mean velocity profiles: $x/c=0.3$; $R_c=1.3\times10^5$; $\alpha=28$ deg; $y/c=0.003$.

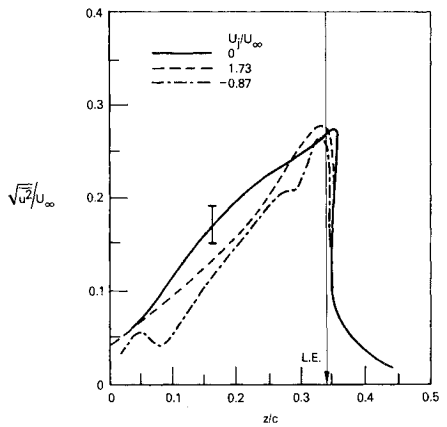

Fig. 9 Effects of suction and ejection on the rms velocity fluctuations: $x/c=0.3$; $R_c=1.3\times10^5$; $\alpha=28$ deg; $y/c=0.003$.

plots of this function for different spanwise locations near the suction surface of the unperturbed delta wing. Figure 10 depicts the probability density function at $x/c=0.6$, $y/c=0.01$ for three spanwise positions very near the leading edge, 1.0 mm and 0.5 mm outward of the edge and 1.0 mm inward from it, corresponding to $z/c=0.349$, 0.348, and 0.344, respectively. The Reynolds number is $R_c=1.3\times10^5$, and the angle of attack is $\alpha=28$ deg. In Fig. 10, the abscissa is the streamwise velocity, and the ordinate is a normalized probability density function such that the area under the curve is unity. Just outside the leading edge ($z/c=0.349$), the discrete vortices manifest themselves as negative spikes in the instantaneous velocity record, and the probability density function is skewed, i.e., the mean (5.64 m/s) and the most probable velocity (5.9 m/s) do not coincide. The local mean velocity is still smaller than the most probable velocity at $z/c=0.348$. However, the opposite is found just inward from the leading edge at $z/c=0.344$, where the most probable velocity is 2.4 m/s and the local mean velocity is 3.37 m/s. The negative and positive skewnesses evident in Fig. 10 are consistent with the negative and positive spikes observed in the instantaneous velocity signals just outward and just inward of the leading edge (Fig. 3).

Similar trends are observed at higher normal positions but with a shifted spanwise position corresponding to the different location of the shear layer. For example, at $y/c=0.03$, low-speed fluctuations are more probable inward of the leading edge ($z/c=0.344$), but this trend reverses further inward at $z/c=0.22$.

Perturbing the leading edge with subharmonic injection of secondary fluid will shift the shear layer and modulate the pairing process as was indicated in the mean and rms velocity profiles shown in Sec. IV. At a fixed position, leading-edge perturbations would correspondingly affect the probability density function. This is demonstrated in Fig. 11 for $U_j/U_\infty=1.73$ with similar run conditions to those depicted in Fig. 10 for the unperturbed case. The probability density function at four spanwise positions is shown in Fig. 11: $z/c=0.345$, 0.344, 0.341, and 0.336 (0.5, 1, 2, and 4 mm inward of the leading edge, respectively). The mean streamwise velocity at the respective positions is 5.59, 5.72, 5.89, and 5.71 m/s, while the most probable velocity is 5.25, 5.2, 5.4, and 5.65 m/s, indicating positive skewness at all four inward locations. The one common position at $z/c=0.344$ in Figs. 10 and 11 illustrates that the mean value of the velocity has been shifted significantly and the rms fluctuation level has been altered by the perturbation.

The narrowness of the probability distributions depicted in Fig. 11 as compared to those shown in Fig. 10 is apparently a direct result of the leading edge excitations and their effects on the bounded shear layer. As was shown in the flow visualization results in Sec. III, subharmonic perturbations at the leading edge lead to more repeatable pairings of the discrete vortices and to a more organized large vortex. The velocity records at points where the discrete vortices are pairing and are dynamically interacting should then manifest a narrower probability distribution.

VI. Spectral Analysis

The autocorrelation and spectrum of the longitudinal velocity fluctuations are two statistical quantities useful in analyzing the discrete vortices shed from the leading edge of the delta wing and the effects of the perturbation device on these vortices. The autocorrelation coefficient is the correlation between the values of the streamwise velocity fluctuations u at two different times nondimensionalized using the mean square:

$$R(\tau)=\overline{u(t)\,u(t-\tau)}/\overline{u^2}$$

where the overbar denotes a time average. The Fourier transform of the autocorrelation coefficient is the power

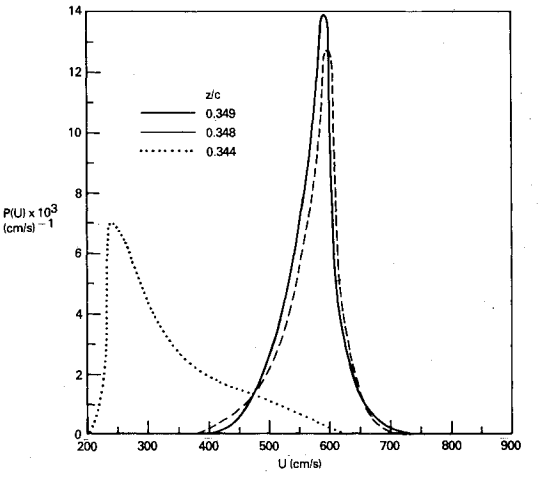

Fig. 10 Spanwise changes of probability density function: $x/c=0.6$; $y/c=0.01$; $R_c=1.3\times10^5$; $\alpha=28$ deg; $U_j/U_\infty=0$.

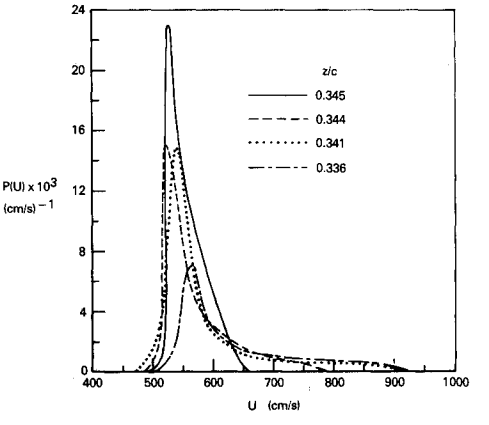

Fig. 11 Spanwise changes of probability density function in the perturbed case: $x/c=0.6$; $y/c=0.01$; $R_c=1.3\times10^5$; $\alpha=28$ deg; $U_j/U_\infty=1.73$.

spectral density:

$$S(f)=\frac{1}{2\pi}\int_{-\infty}^{\infty}e^{-2\pi\tau f}R(\tau)\,d\tau$$

which is the normalized spectral distribution of the squared intensity of the longitudinal velocity fluctuations.[16] These two functions provide a convenient method of determining length scales in the flowfield and may provide clues to periodic and/or other structures embedded in the random velocity fluctuations.

The effects of leading edge perturbations on the dimensional spectral distribution [$S'(f)=\overline{u^2}S(f)$] are shown in Fig. 12 at the three spanwise positions $z/c=0.345$, 0.344, and 0.22. Other run conditions are $x/c=0.6$, $y/c=0.03$, $R_c=1.3\times10^5$ and $\alpha=28$ deg. In the perturbed case, the ejection velocity was $U_j=1.73\ U_\infty$, and the frequency was the first subharmonic. The spectral peak evident in the figure corresponds to the natural shedding frequency of 37 Hz and is relatively unchanged by the forcing. In the unperturbed case, the peak is more dominant near the leading edge and decays inboard. For the three spanwise locations progressively inboard of the leading edge, the mean square of the streamwise velocity fluctuations was 1.19, 1.30, and 0.59 m^2/s^2 in the unperturbed case and 0.52, 1.25, and 1.85 m^2/s^2 in the perturbed case, consistent with the variations in the area under each curve depicted in Fig. 12.

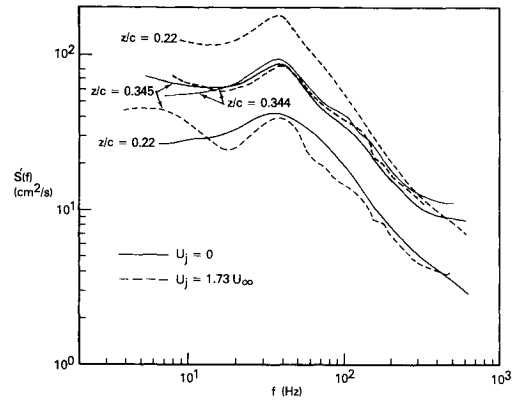

Fig. 12 Effects of leading edge perturbations on longitudinal velocity spectrum: $x/c=0.6$; $y/c=0.03$; $R_c=1.3\times10^5$; $\alpha=28$ deg.

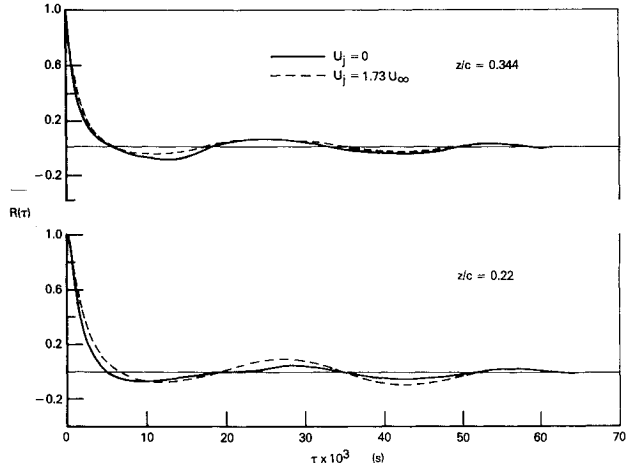

Fig. 13 Autocorrelation coefficient with and without leading edge excitations: $x/c=0.6$; $y/c=0.03$; $R_c=1.3\times10^5$; $\alpha=28$ deg.

At the higher elevation, $y/c=0.08$, the spectral peak was almost nonexistent at $z/c=0.334$ and increased inboard to form a predominate peak at $z/c=0.308$. These results are consistent with the general outline of the shear layer revealed from the flow visualization experiments and the mean velocity profiles.

The correlation coefficients did not show significant changes when the forcing was applied consistent with the fact that the shape of spectra is similar at these locations. Examples at $x/c=0.6$ and $y/c=0.03$ are found in Fig. 13 for two spanwise locations; $z/c=0.344$ and 0.22. The remaining parameters are identical to those of Fig. 12. The period of oscillation in the autocorrelation coefficient (27 ms) corresponds to the natural shedding frequency of the leading-edge vortices, while the first zero crossing is proportional to the value of the integral time scale. The forcing effects are more pronounced further inboard from the leading edge at $z/c=0.22$. The slightly larger secondary negative peak in the perturbed case at $\tau\simeq0.043$ s indicates more evidence of the subharmonic when the forcing is applied.

At $y/c=0.005$ and outboard of the leading edge at $z/c=0.351$, a strong secondary positive peak of 0.2 appeared in the autocorrelation coefficient at $\tau=0.025$ s, implying strong irrotational fluctuations there. The first zero crossing occurred at $\tau=15$ ms but decreased to about 6 ms at $z/c=0.344$, indicating a gradual decrease in the integral time scale.

VII. Summary

Based on our recent discovery that a leading-edge vortex on a delta wing in steady flight consists of a series of discrete smaller vortices, a perturbation of these discrete vortices was studied. The perturbed and unperturbed flowfields around a delta wing at constant angle of attack were measured experimentally in a water towing tank and a low-speed wind tunnel. Flow visualization and fast-response velocity probe surveys were conducted to study the shear layer formed on the suction side of the wing and to determine the effects of periodic suction or ejection from a leading-edge slot on the shedding and pairing of the discrete vortices.

The flow visualization experiments showed that periodic injection from a leading-edge slot significantly changed the shear layer on the suction side of the wing. A subharmonic perturbation at a relatively low amplitude seemed to enhance the pairing process and resulted in a more organized large vortex.

Miniature hot-wire probes were used to survey the instantaneous streamwise velocity at different positions within the leading-edge vortices in the wind tunnel. The instantaneous signals clearly showed positive and negative velocity spikes consistent with the passing of the shed vortices by the fixed probe; thus further confirming our previous flow visualization findings regarding the discrete nature of the leading edge vortices. Leading edge perturbations dramatically affected the intense shear layer as evidenced by the marked changes in the different statistical quantities.

The mean flowfield showed a significant change when the forcing was applied. This alteration was greatest slightly inboard of the leading edge as seen by comparing Figs. 4 and 6. The rms distribution of the streamwise velocity fluctuations was also dramatically altered, as shown in Figs. 5 and 7. The intense fluctuations appeared to be more confined to the leading-edge region with the forcing. The excitation also affected other statistical quantities such as the probability distributions and spectra.

Some of the results illustrate dramatic changes in the mean and rms profiles. For example, Figs. 4 and 6 show that the perturbation greatly decreases the (dimensionless) mean velocity at $x/c=0.6$ from extremes of 0.6–2.0 without perturbation to 1.0–1.4 with leading-edge excitations; whereas in Fig. 8 the disturbance increases the extremes in a comparable manner at $x/c=0.3$. Similarly at $z/c=0.2$, Figs. 5 and 7 show that the subharmonic perturbation reduces the rms level at $y/c=0.01$ from 0.2 to less than 0.05; whereas the spectra in Fig. 12 illustrate an *increase* in the rms level at $y/c=0.03$. The leading-edge perturbation undoubtedly affects both the main vortex and the secondary separation region. More complete documentation of the complex flowfield is needed, however, before the two effects can be segregated.

The complexity of the three-dimensional flowfield under consideration is evident from the mean and rms velocity profiles shown in Figs. 6 and 7. While measurements of the streamwise velocity component give some indication of the flowfield, complete documentation of all three velocity components is essential for understanding the complex flow. Also, aerodynamic forces must be measured to document the effects of leading-edge excitations on the lift, drag and moments.

A very important, and still unanswered question, is whether or not the discrete model of leading edge vortices evident from the present qualitative and quantitative data is valid at flight Reynolds number and Mach number. A definitive answer must, of course, await further high-speed experiments. However, it is our belief, based on the data presented in this paper, that the development of the leading-edge vortices on a delta wing is very similar to the development of a two-dimensional mixing layer downstream of a splitter plate. In the latter case, the basic vorticity distribution possesses a maximum and is inviscidly unstable to small pertubations via the Kelvin-Helmholtz instability mechanism. Thus, two-dimensional waves grow exponentially with downstream distance and are observed to roll up into discrete vor-

tices, regardless of the Reynolds number. According to Ho and Huerre,[12] the evolution of vortical structures in both laminar and turbulent mixing layers is governed by essentially the same dynamic processes. Interacting spanwise vortices have been observed not only in the early laminar stages of the free shear layer evolution but also farther downstream in the turbulent region, where they coexist with a fine-scale motion. These features have been observed experimentally[17] up to values of the Reynolds number at least as high as 10^7.

The main conclusion from the present study is that the bound vortices that produce the nonlinear lift on delta wings can be significantly altered by applying velocity perturbations near the leading edge. This technique may be useful for changing the vortex structure and hence provide a unique means of aerodynamic control. Although not considered in the present investigation, the subharmonic leading edge perturbations may also have significant effects on the phenomenon of vortex bursting occurring at large angles of attack. By properly choosing the periodic injection's frequency and amplitude, the leading-edge vortex breakdown may be delayed or enhanced as required.

Acknowledgments

This work is supported by the Air Force Office of Scientific Research under Contract F49620-85-C-0131 and monitored by Dr. James D. Wilson. The authors would like to acknowledge the valuable help of Miles Ashley, Robert Breidenthal, Scott Brown, Luke Shindo, and Randy Srnsky.

References

[1]Herbst, W. B., "Supermaneuverability," in *Unsteady Separated Flows,* edited by M. S. Francis and M. W. Luttges, University of Colorado, Boulder, Aug. 1983, pp. 1–9.

[2]Herbst, W. B., "Dynamics of Air Combat," *Journal of Aircraft*, Vol. 20, July 1983, pp. 594–598.

[3]Elle, B. J., "An Investigation at Low Speed of the Flow Near the Apex of Thin Delta Wings with Sharp Leading Edges," Aeronautical Research Council, R&M 3176, Jan. 1958.

[4]Wentz, W. H., Jr. and Kohlman, D. L., "Wind Tunnel Investigations of Vortex Breakdown on Slender Sharp-Edged Wings," NASA CR-98737, Nov. 1968.

[5]Werlé, H., "Hydrodynamic Flow Visualization," *Annual Review of Fluid Mechanics*, Vol. 5, Jan. 1973, pp. 361–382.

[6]Hoerner, S. F. and Borst, H. V., *Fluid Dynamic Lift,* L. A. Hoerner, Brick Town, NJ, 1975.

[7]Faery, H. F. Jr., Strozier, J. K., and Ham, J. A., "Experimental and Theoretical Study of Three Interacting, Closely-Spaced, Sharp-Edged 60° Delta Wings at Low Speeds," NASA CR-3460, 1981.

[8]Gad-el-Hak, M. and Blackwelder, R. F., "The Discrete Vortices from a Delta Wing," *AIAA Journal*, Vol. 23, June 1985, pp. 961–962.

[9]Winant, C. D. and Browand, F. K., "Vortex Pairing: The Mechanism of Turbulent Mixing-Layer Growth at Moderate Reynolds Number," *Journal of Fluid Mechanics*, Vol. 63, April 1974, pp. 237–255.

[10]Brown, G. L. and Roshko, A., "On Density Effects and Large Structure in Turbulent Mixing Layers," *Journal of Fluid Mechanics*, Vol. 64, July 1974, pp. 775–816.

[11]Roshko, A., "Structure of Turbulent Shear Flows: A New Look," *AIAA Journal*, Vol. 14, Oct. 1976, pp. 1349–1357.

[12]Ho, C.-M. and Huerre, P., "Perturbed Free Shear Layers," *Annual Review of Fluid Mechanics*, Vol. 16, Jan. 1984, pp. 365–424.

[13]Gad-el-Hak, M., Blackwelder, R. F., and Riley, J. J., "On the Growth of Turbulent Regions in Laminar Boundary Layers," *Journal of Fluid Mechanics,* Vol. 110, Sept. 1981, pp. 73–95.

[14]Lumley, J. L., *Stochastic Tools in Turbulence*, Academic Press, New York, 1970.

[15]Tennekes, H. and Lumley, J. L., *A First Course in Turbulence,* MIT Press, Cambridge, MA, 1972.

[16]Hinze, J. O., *Turbulence*, 2nd ed., McGraw-Hill, New York, 1975.

[17]Dimotakis, P. E. and Brown, G. L., "The Mixing Layer at High Reynolds Number: Large-Structure Dynamics and Entrainment," *Journal of Fluid Mechanics*, Vol. 78, Dec. 1976, pp. 535–560.